Low-temperature sintering of dense lanthanum silicate electrolytes with apatite-type structure using an organic precipitant synthesized nanopowder

Seung Hwan Jo,[a] P. Muralidharan,[a] and Do Kyung Kim[b]
Department of Materials Science and Engineering, Korea Advanced Institute of Science and Technology (KAIST), Yuseong-gu, Daejeon 305-701, Republic of Korea

(Received 19 March 2008; accepted 8 October 2008)

Highly sinterable $La_{10}Si_6O_{27}$ and $La_{10}Si_{5.5}M_{0.5}O_{27}$ (M = Mg, and Al) nanopowders with apatite-type structure have been synthesized via a homogeneous precipitation method using diethylamine (DEA) as a precipitant. The synthetic approach using an organic precipitant with dispersant characteristics is advantageous in configuring weakly agglomerated nanopowders, leading to desirable sintering activity. X-ray diffraction powder patterns confirmed the single-phase crystalline lanthanum silicate of hexagonal apatite structure at 800 °C, which is a relatively lower calcination temperature compared to conventionally prepared samples. Transmission electron microscopy images revealed particles ~30 nm in size with a high degree of crystallinity. A dense grain morphology was recognized from the scanning electron microscopy images of the polished surface of the pellets that were sintered at 1400 and 1500 °C for 10 h. This low-temperature sintering is significant because conventional powder processing requires a temperature above 1700 °C to obtain the same dense electrolyte. The doped-lanthanum silicate electrolyte prepared by the DEA process and sintered at 1500 °C for 10 h exhibited electrical conductivity comparable with samples prepared at much higher sintering temperature (>1700 °C).

I. INTRODUCTION

Intermediate-temperature solid oxide fuel cells (IT-SOFCs), which have operating temperatures ranging from 400 to 700 °C, have come to be considered state-of-the-art in the area of power fabrication. This is because of their long-term stability and cost saving potential when produced as large units.[1–3] Until recently, conventionally used solid electrolytes with high ionic conductivity consisted of fluorite-structured stabilized zirconia, which requires an operating temperature above 900–1000 °C.[4–7] Therefore, serious attention has been paid to finding alternative electrolytes for IT-SOFCs, which has led to the development of fluorite and perovskite structures, such as doped ceria and doped lanthanum gallate, respectively.[3,4,8–11] However, the application of those materials has been limited by the increase in the electronic conductivity, which occurs in doped-ceria-based electrolytes and by the insufficient chemical stability that characterizes doped lanthanum gallate materials.[12]

Lanthanum silicate-based compositions that have an apatite-type structure and high electric conductivity have recently attracted significant interest. Initially, Nakayama et al. reported that $Ln_{10-x}Si_6O_{26+y}$ (Ln = La, Sm, Nd, Dy, Gd, x = 8 to 11) materials with an apatite structure exhibited ionic conductivity.[13,14] Among the lanthanum silicate apatite solid electrolytes, the composition of $La_{10}Si_6O_{27}$ has exhibited high oxygen ionic conductivity of $>10^{-3}$ Scm^{-1} at 500 °C, which is comparably higher than that of 8 mol% yttria doped zirconia (YSZ) electrolytes.[13,15] In addition, it has been reported that these lanthanum silicate materials have high oxygen ion transference numbers (>0.9) over a wide range of oxygen partial pressures.[16–18] Furthermore, aliovalent doping onto Si sites is effective at enhancing electrical conductivity.[17,19,20] The apatite structure consists of isolated tetrahedral SiO_4 units with rare-earth cations located in two cavity sites of the seventh coordinated and the ninth coordinated of the crystal. The remaining oxide ions reside in one-dimensional channels associated through the structure. As a result, high ionic conduction has been reported via an interstitial pathway mechanism, which is in contrast to the oxide ion vacancy mechanism in perovskite and fluorite-type oxide ion conductors.

[a]These authors contributed equally to this work.
[b]Address all correspondence to this author.
e-mail: dkkim@kaist.ac.kr
DOI: 10.1557/JMR.2009.0018

Even though $La_{10}Si_6O_{27}$ compositions have been reported to possess high electrical conductivity, difficulty exists in obtaining samples with a pure single phase and high densification below 1700 °C. The most common impurity phases identified in the $La_{10}Si_6O_{27}$ pellets sintered below 1775 °C include $La_{9.33}Si_6O_{26}$ and La_2SiO_5 phases. Bondar et al.[21] reported that, in the La_2O_3–SiO_2 phase diagram, the $La_{9.33}Si_6O_{26}$ composition has been shown to yield relatively lower electrical conductivity compared with $La_{10}Si_6O_{27}$, in spite of having a very similar lattice structure.[13,22] Therefore, the development of feasible synthesis methods for obtaining highly sinterable $La_{10}Si_6O_{27}$ powders may facilitate the use of lanthanum-silicate-based materials as promising solid electrolytes for IT-SOFCs.

A conventional solid-state reaction was used to prepare the lanthanum silicate electrolytes. This involved prolonged high sintering temperatures that were above 1700 °C to obtain full densification and a pure single-phase compound. In this reaction, despite the high sintering temperature, surplus impurity phase formation occurs. This includes the formation of $La_{9.33}Si_6O_{26}$, and La_2SiO_5, which tends to greatly retard the electrical conductivity.[17,19,23,24] It has subsequently been recognized that the solution-based synthesis of single- or multi-oxide powders results in high sintering activities, high surface areas, well-defined chemical compositions, and a homogeneous distribution of the elements. Shanwen Tao et al.[22] and Changan Tian et al.[25] reported the synthesis of $La_{9.33}Si_6O_{26}$ and $La_{10}Si_6O_{27}$ nanopowders through a sol-gel process. Even after a prolonged heating profile at 1400 °C their results showed poor densification, which was below 80% the theoretical.

Therefore, it has become a challenging task for researchers to find a better synthesis process for obtaining nanocrystalline lanthanum silicate electrolyte powders with good sintering activity and high electrical conductivity. According to conventional sintering theory, nanocrystalline powders show higher sinterability compared with coarse powders due to their high driving force for lowering surface free energy, which leads to the enhancement of densification.[26,27] In addition, weak agglomeration and homogeneous granules of nanopowders have been recognized as crucial factors in producing highly densified pellets.[28,29] In the literature, it has been reported that nanocrystalline powders synthesized via the alkoxide process in organic solvents normally show higher reactivity and weak agglomeration during the drying stage. This evidently results in better dispersion and high sinterability.[28] Similarly, in this process, most metal nitrate hydrates and some organic precipitants such as diethylamine are dissolved into alcohols. The precipitating anions (OH^-) are then generated by the hydrolysis of precipitant with the molecular water of the metal salts.[29] As a result, a minimum amount of water is involved, similar with the alkoxide method, in which the resultant powders showed better dispersion.

The present work describes a simple and effective procedure for synthesizing single-phase, weakly agglomerated nanopowder with high crystallinity of $La_{10}Si_6O_{27}$ and $La_{10}Si_{5.5}M_{0.5}O_{27}$ (M = Mg, and Al) electrolytes via a DEA precipitation process. The effect of a sintering temperature range of 1200–1600 °C for high densification was investigated. Electrical properties were investigated through impedance analysis as a function of temperature in air and were compared with reports in the literature.

II. EXPERIMENT AND METHODS

The precursor materials used for the synthesis were $La(NO_3)_3{\cdot}6H_2O$, $Mg(NO_3)_2{\cdot}6H_2O$ $Al(NO_3)_3{\cdot}9H_2O$ (>99.999%, Aldrich, St. Louis, MO) and tetraethyl orthosilicate [TEOS; $Si(OC_2H_5)_4$, > 99.997%, Aldrich], diethylamine [(DEA; $(C_2H_5)_2NH$, 99.9%, Aldrich], absolute ethanol (Baker, Phillipsburg, NJ), and de-ionized (DI) water, which was DI with a Millipore Milli Q system (Waters, Milford, MA). The chemicals were used as received without further purification.

A versatile precipitation process was introduced using DEA as a precipitant to prepare the nanocrystalline $La_{10}Si_6O_{27}$ powder. In a typical procedure, 3.125 mM $La(NO_3)_3{\cdot}6H_2O$ and 1.875 mM TEOS were dissolved in 50 mL ethanol separately with continuous stirring to form a clear homogenous solution. The above two solutions were mixed together and homogenized with continuous stirring for 1 h at room temperature. To the clear solution above, 0.25 mol DEA was added drop-wise with vigorous continuous stirring. The solution immediately turned into a thick whitish slurry, which was further stirred in the same vigorous manner and precipitated. A small amount of DI water was added to the precipitate and allowed to stand for a few hours to ensure complete precipitation. After the reaction, the final products were washed systematically with DI water and ethanol by centrifugation. The white powder obtained was subsequently dried at 60 °C for 12 h and calcined at 400, 700, and 800 °C for 10 h. The phase formation behavior was examined. The chemical reactions can be expressed by the following equation:

$$10\ La(NO_3)_3\ 6H_2O + 6\ Si(OC_2H_5)_4 \xrightarrow[(RT)]{} y(C_2H_5)_2NH/C_2H_5OH\ \ [\text{intermediate complex step}] \xrightarrow[(RT)]{}$$
$$(x)\ La_{10}Si_6(OH)_{54}{\cdot}nH_2O_{(amorphous)} + (1-x)\ La_{10}Si_6O_{27}{\cdot}nH_2O_{(amorphous)} + y(C_2H_5)_2NH_2NO_3 + nH_2O \quad . \qquad (1)$$

In the expected chemical reaction, the intermediate steps involve complex formation via the hydrolysis and co-precipitation of TEOS and $La(NO_3)_3$ in the presence of DEA as a precipitant in an ethanol medium. The precipitant DEA plays a significant role in forming hydrogen bonds with the hydrated water of the metal salts and exhibits a strong inclination to acquire protons from the hydroxide complexes. This is a crucial stage in the process of DEA as a precipitant for the preparation of weakly agglomerated and homogenously dispersed particles of mixed $La_{10}Si_6(OH)_{54}\cdot nH_2O$ and $La_{10}Si_6O_{27}\cdot nH_2O$ amorphous powders.

The powder that was calcined at 800 °C was ball milled for 24 h in ethanol with zirconia media. After subsequent drying and granulation, the powder was uniaxially pressed, followed by cold isostatic presses (CIP) under 200 MPa. The $La_{10}Si_6O_{27}$ pellets were sintered in an electric furnace at 1200, 1300, 1400, 1500, and 1600 °C for 10 h in air with a heating ramp of 5 °C min^{-1}. The above synthesis procedure was followed to produce $La_{10}Si_{5.5}Al_{0.5}O_{27}$ and $La_{10}Si_{5.5}Mg_{0.5}O_{27}$ electrolytes, which were sintered at 1500 °C for 10 h.

The synthesized samples were characterized using an x-ray diffractometer (D/MAX-IIIC x-ray diffractometer, Rigaku, Tokyo, Japan) with Cu Kα radiation (40 kV and 45 mA). The as-synthesized $La_{10}Si_6O_{27}$ nanopowder was analyzed via thermal analysis (TG/DTA; TA, SDT Q600 V 8.3, Newcastle, DE) in air at a heating rate of 10 °C min^{-1} to investigate its decomposition and crystallization behaviors. The particle morphology and crystallinity were characterized using transmission electron microscopy (TEM; TEM 3010, JEOL, Tokyo, Japan) with an accelerating voltage of 300 kV. The relative density of the samples, which experienced different sintering conditions, was measured using the Archimedes method in DI water. The dense $La_{10}Si_6O_{27}$ pellet was polished and then underwent thermal etching at 100 °C lower than the sintering temperatures to which the respective samples were exposed. The grain morphology of the dense pellets was characterized using a scanning electron microscope (FE-SEM; Philips XL30 FEG, Eindhoven, The Netherlands).

To perform impedance analysis, the surfaces of the sintered pellets were polished. Platinum paint was then applied to either side of the pellets, which were then heat treated at 1000 °C for 1 h to achieve stable contact of the electrode to the pellet surfaces. The platinum-electrode-coated pellet was then attached to a platinum mesh, which was connected with platinum wires and sandwiched in a spring-loaded specimen holder. The electrical conductivity of the pellets was studied in the presence of air by alternating current (ac) impedance spectroscopy (Solartron 1260 impedance/gain-phase analyzer, Farnborough, UK), which was interfaced with a computer-controlled program for data acquisition. The impedance spectra were measured over the frequency range of 1 Hz to 10 MHz as a function of temperature from 350 to 700 °C.

III. RESULTS AND DISCUSSION

A. XRD

The XRD patterns of the $La_{10}Si_6O_{27}$ sample in Fig. 1 show the as-synthesized, calcined powders at 400 and 800 °C and a sintered pellet at 1400 °C, synthesized via the DEA process. The XRD patterns of the as-synthesized powders at room temperature (RT), which were calcined at 400 °C and 700 °C showed a clear amorphous phase. The powders calcined at 800 °C and above revealed the formation of a crystalline single phase of $La_{10}Si_6O_{27}$ with a hexagonal apatite-type structure. The sintered pellet at 1400 °C showed a single-phase with high degree of crystallinity. The patterns of $La_{10}Si_6O_{27}$ are well-matched with JCPDS No. 53-0291. In Fig. 1, the powder calcined at 800 °C exhibited a smaller crystallite size of 23.24 nm, as calculated from the Scherrer equation, $D = (0.9\lambda)/(\beta\cos\theta)$, where D is the crystallite size, λ is the wave length of incident x-rays (0.15406 nm), β is the half-width full maximum, and θ is the diffraction angle. Thus, the nanopowders synthesized via the DEA process showed a single-phase of $La_{10}Si_6O_{27}$ that formed at a lower calcination temperature of 800 °C, which led to the formation of the weakly bonded nano particles for higher sintering activity.

B. TG/DTA

The thermal analysis data for the as-synthesized $La_{10}Si_6O_{27}$ nanopowder from the DEA process are shown in Fig. 2. The TG curve shows a weight loss of 21.4% up to 700 °C for the as-synthesized $La_{10}Si_6O_{27}$

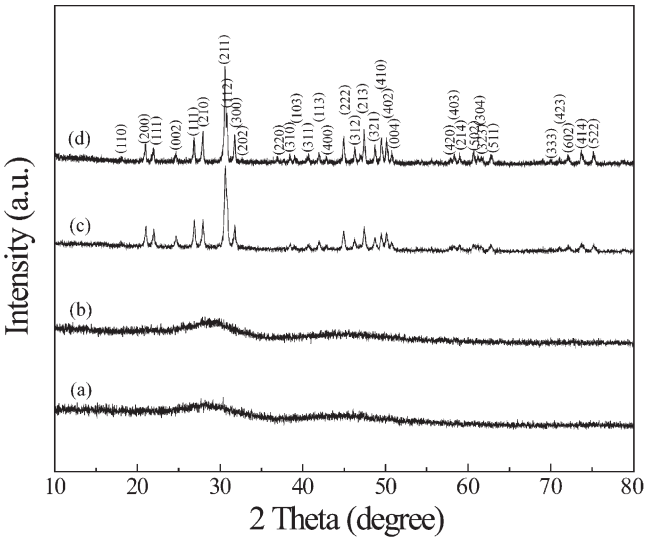

FIG. 1. X-ray diffraction patterns of the $La_{10}Si_6O_{27}$ (a) as-synthesized and (b) calcined nanopowders at 400 °C and (c) 800 °C; and (d) sintered pellet at 1400 °C for 10 h.

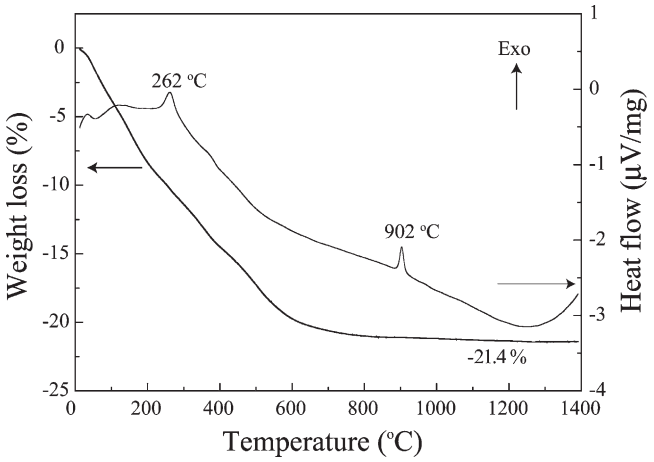

FIG. 2. TG/DTA curves of the as-synthesized $La_{10}Si_6O_{27}$ nanopowder.

nanopowder from the DEA precipitation. The weight loss may be attributed to the dehydration and decomposition of organic residuals. The two small but notable exothermic peaks were observed in the heat flow curve; the peak around 262 °C may be attributed to the decomposition of residual $(C_2H_5)_2NH_2NO_3$ into gaseous phases, and the peak at 902 °C may be due to crystallization of an apatite-type $La_{10}Si_6O_{27}$ phase.[22,29]

C. TEM

Figure 3 shows bright-field and high-resolution (HR) TEM images for the $La_{10}Si_6O_{27}$ nanopowder synthesized by the DEA process and calcined at 800 °C for 10 h. The images clearly show round-shaped, homogenously dispersed $La_{10}Si_6O_{27}$ nanoparticles of a size around 30 nm. The HRTEM micrograph revealed nanocrystalline particles with well-defined lattice planes of 4.22Å spacing, corresponding to the interplanar distance of (211) planes, which demonstrated the high degree of crystallinity of the formed apatite $La_{10}Si_6O_{27}$ phase with regular periodicity of the lattice. Thus, the high-crystalline single-phase powders produced at a lower calcination temperature of 800 °C are a considerable advantage of the DEA process compared with conventional processes.[13,22] The HRTEM and the XRD patterns (Fig. 1) clearly revealed that the DEA process can facilitate synthesis of nano-sized $La_{10}Si_6O_{27}$ particles with homogenous dispersion and a high degree of crystallinity at 800 °C for 10 h.

D. Density and SEM

Figure 4 shows the sintering behavior of the $La_{10}Si_6O_{27}$ pellets sintered at 1200, 1300, 1400, 1500, and 1600 °C from the nanopowder calcined at 800 °C for 10 h. The $La_{10}Si_6O_{27}$ pellets sintered at temperatures of 1200 and 1300 °C showed a density of 67% and 78%, respectively, whereas those sintered in the temperature

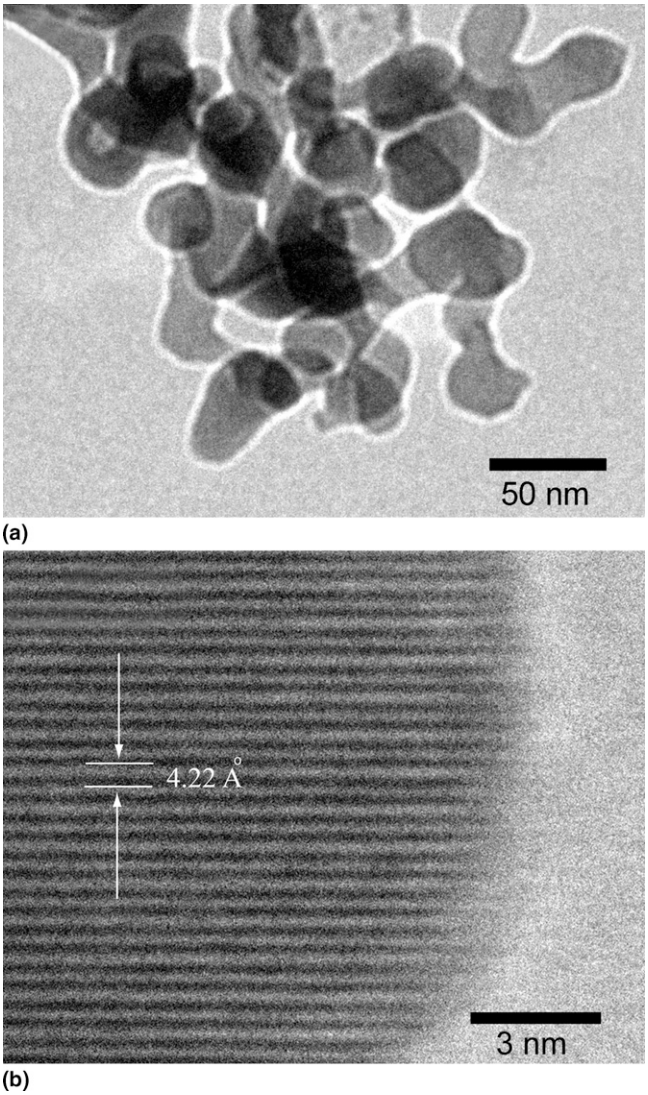

FIG. 3. Bright-field TEM and HRTEM images of the $La_{10}Si_6O_{27}$ nanopowder synthesized via the DEA process and calcined at 800 °C.

range from 1400 to 1600 °C showed a relatively high density, which was above 95% theoretical density. The distinct high relative density of above 95% was achieved due to the weakly agglomerated nanoparticles of $La_{10}Si_6O_{27}$ with a high degree of crystallinity, which were synthesized via the DEA process and calcined at a low-temperature of 800 °C. In the literature,[26–29] it has been clearly demonstrated that particle size plays a significant role in influencing the sintering behavior of ceramic materials. Thus, nanopowders with desirable sintering activity have allowed sintering that uses a dwelling period of 10 h, which is shorter than the conventional dwelling period. They have also allowed sintering at a temperature of 1400 °C, which is about 300 °C lower than that which is used in conventional sintering. Tao et al.[22] reported that the relative densities for $La_{10}Si_6O_{27}$ sintered at 1400 °C for a 20 h period and

for a three day period have resulted in lower densification of 69% and 74%, respectively. In addition, increasing the sintering temperature to 1500 °C for 22 h has resulted in a density of only 80% theoretical density, which is not sufficient for obtaining highly sintered pellets that possess the high electrical property of solid electrolytes. Even though the primary particle size is quite small, densification can be retarded by strong agglomeration and inhomogeneous compaction of the nanopowders. Thus, good dispersion and homogenization compaction are crucial to maximizing the high densification nature of nanoparticles. In this study, weakly agglomerated reactive nanoparticles with characteristic properties have been synthesized through the DEA precipitation process. Table I presents the sintering conditions for fully densified $La_{10}Si_6O_{27}$ pellets obtained from a simple and economic precipitation process using DEA as a precipitant, which allows for a lower sintering temperature compared with that which has been reported in the literature.

Figure 5 shows SEM images for the polished surfaces of $La_{10}Si_6O_{27}$ pellets sintered at 1200, 1300, 1400, and 1500 °C for 10 h. The SEM images of sintered pellets at 1200 and 1300 °C clearly demonstrate the porous microstructures with approximately 33% and 22% porosity, respectively. The micrograph image of sintered pellets at 1400 and 1500 °C exhibited highly dense grains and distinctly resolved grain boundaries with negligible porosity, which are the typical microstructural features of highly densified pellets [Figs. 5(c) and 5(d)]. The sintered pellet with a high density of above 95%, as determined by the Archimedes' method, is shown in the dense microstructure images in Figs. 5(c) and 5(d). The average size of grains in sintered pellets ranges from 500 nm to 1 μm. The sintered pellets at 1400 and 1500 °C showed normal grain growth behavior. These results indicate that the high sinterability at low temperature could be attributed to the homogeneous dispersion of particles, small crystallite size, and weak agglomeration of the calcined nanopowders synthesized by the DEA process, as evidenced by XRD and TEM analysis.

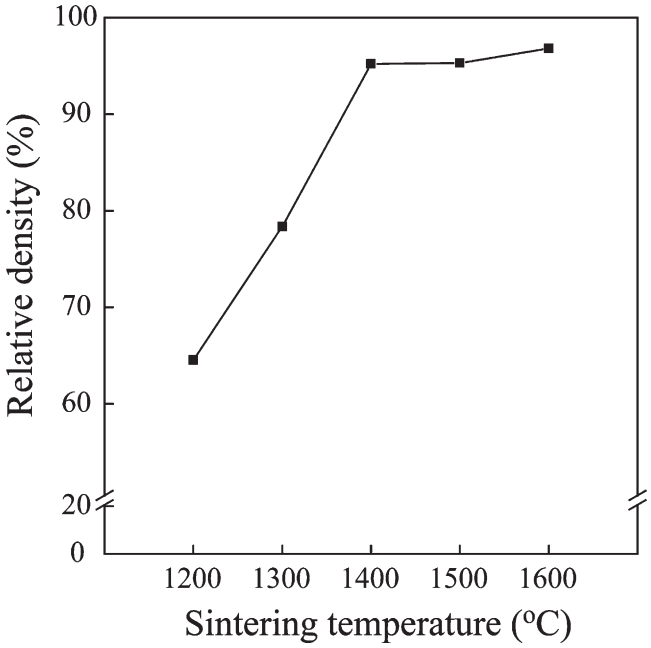

FIG. 4. Relative density of the $La_{10}Si_6O_{27}$ nanopowders sintered at 1200, 1300, 1400, 1500, and 1600 °C for 10 h using the nanopowder calcined at 800 °C for 10 h.

E. Electrical transport property

Figures 6(a) and 6(b) show representative complex impedance spectra for the $La_{10}Si_6O_{27}$ pellet sintered at 1400 °C and measured at 350 and 600 °C in air, respectively. In Fig. 6(a), the evident presence of a depressed semicircle at a high-frequency range is probably due to the resistance of a small bulk (R_b) contribution, and the dominant large depressed semicircle in the middle-frequency region is due to the resistance of grain boundary (R_{gb}) response. The low-frequency region of the spectrum may be attributed to electrode resistance (R_{elect}). The impedance spectrum at 600 °C exhibits one distinct depressed semicircle due to the grain boundary response and a low-frequency spectrum due to the electrode. It can be clearly observed that the semicircles in the spectrum shift to higher frequencies with increasing temperature. The total resistance (R_t) was obtained by fitting the impedance data with an equivalent circuit model (Fig. 6) using an Z-plot program. The inset in Fig. 6 shows a schematic plot of an idealized impedance spectrum and an equivalent circuit model, which is composed of two serial resistance parallel with capacitance (RC) elements. As is clear from the impedance

TABLE I. Comparison of sintering condition and relative density of the sintered lanthanum silicate pellets synthesized via the DEA process with the literature reports.

Composition	Processing	Sintering condition	Relative density (%)	Reference
$La_{10}Si_6O_{27}$	DEA precipitation	1400 °C, 10 h	>95%	This study
$La_{10}Si_6O_{27}$	Solid state reaction	1700 °C, 2 h	...	13
$La_{9.33}Si_6O_{26}$	Solid state reaction	1700 °C	~95%	31
$La_{10}Si_6O_{27}$	Sol-gel process	1400 °C, 20 h	69%	22
$La_{9.33}Si_6O_{26}$	Sol-gel process	1500 °C, 10 h	90%	25

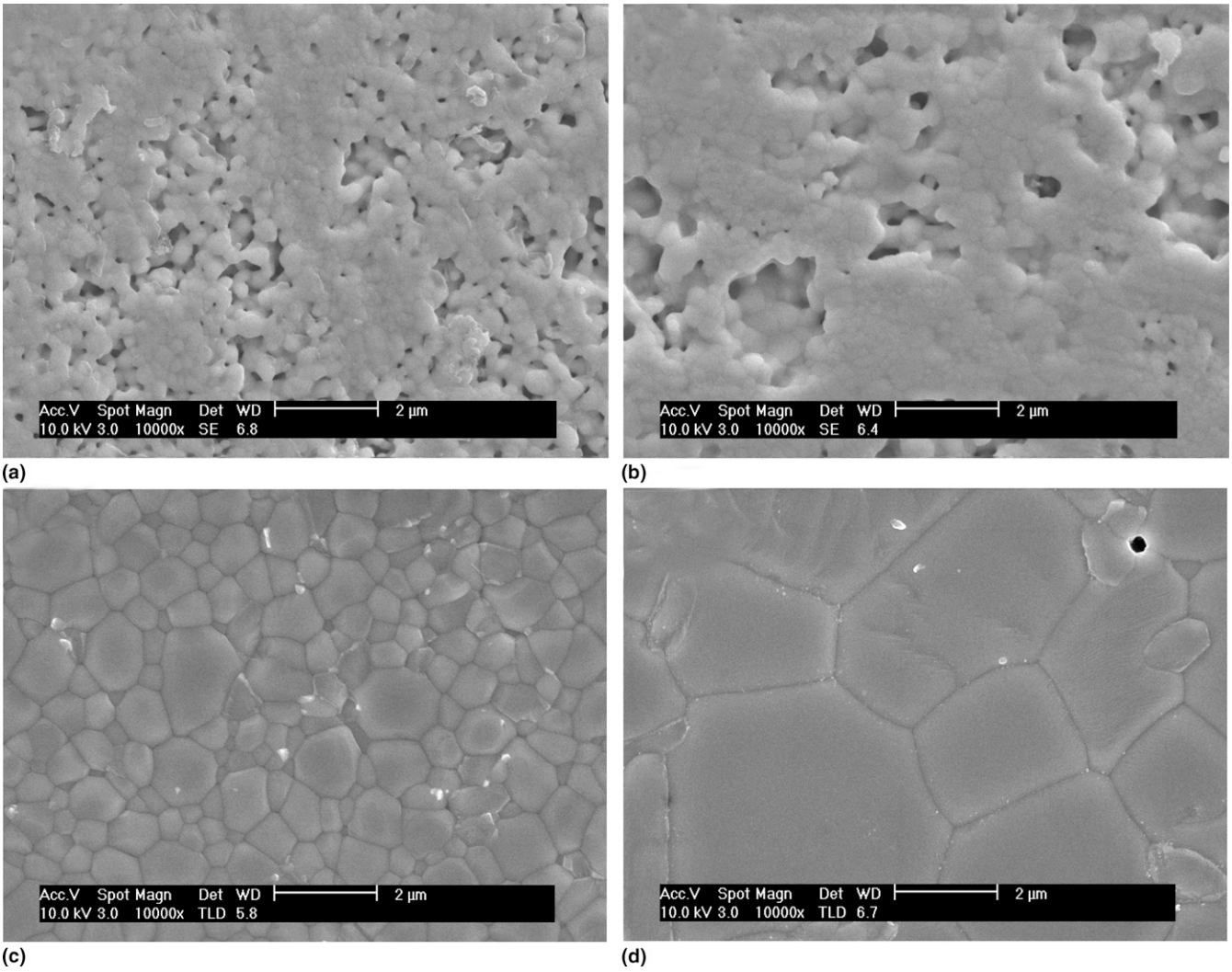

FIG. 5. SEM micrographs of polished surfaces of the $La_{10}Si_6O_{27}$ pellets sintered at (a) 1200 °C, (b) 1300 °C, (c) 1400 °C, and (d) 1500 °C for 10 h.

spectra, the semicircles are depressed, and hence a constant phase element (CPE) is used instead of pure capacitance, as shown in the inset of Fig. 6(a). The impedance spectra were fit with an equivalent circuit with two serial (R parallel with CPE) elements, of which one represents the bulk and the other is related with the grain boundary of the material. The electrode polarization at low-frequency can be modeled by CPE_{elect}. Such a simple model perfectly matches the doped and undoped materials in the entire temperature range. The total resistance of the electrolyte is shown by $R_t = (R_b) + (R_{gb})$. Accordingly, the total electrical conductivity (σ_t) was calculated using the pellets' dimensions and R_t of the samples. Figure 7 shows the calculated total electrical conductivity as a function of temperature following the Arrhenius law in the following equation:

$$\sigma = (\sigma_0/T)\exp(-E_a/RT) \quad , \qquad (2)$$

for the $La_{10}Si_6O_{27}$ sintered at 1400 and 1500 °C, and $La_{10}Si_{5.5}Al_{0.5}O_{26.75}$, and $La_{10}Si_{5.5}Mg_{0.5}O_{26.75}$ pellets sintered at 1500 °C. The obtained conductivity data were compared with those of 8 mol% yttria doped ZrO_2 (YSZ)[30] and literature-reported conductivities of lanthanum silicate electrolytes.[13,22,25,31] The obtained data indicate that substituting Al and Mg into the Si sites leads to a 0.2–0.3 order of increase in the electrical conductivity compared to that of $La_{10}Si_6O_{27}$ pellets. This confirms the utility of the DEA process in obtaining a homogenous solid solution upon doping into the Si sites of lanthanum silicate electrolytes. Table II presents the comprehensive conductivity data and the activation energy data obtained for the undoped and doped lanthanum silicate pellets at different sintering conditions. The best electrical conductivity and the lower activation energy were observed in the $La_{10}Si_{5.5}Al_{0.5}O_{26.75}$ pellet.

The electrical conductivity of low-temperature-sintered undoped- and doped-lanthanum silicate pellets in Fig. 7 illustrated comparable conductivity with that of the YSZ electrolyte. On the other hand, the present data revealed relatively lower conductivity values by half an order

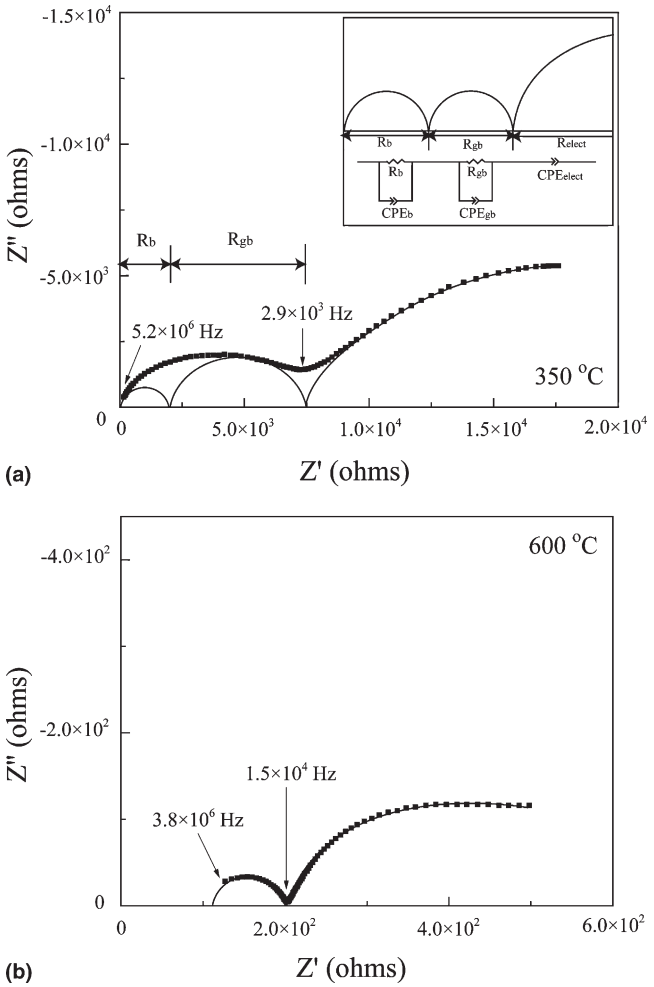

FIG. 6. Impedance spectra of the sintered $La_{10}Si_6O_{27}$ pellet, measured at (a) 350 °C and (b) 600 °C. Inset in (a) shows an idealized impedance spectrum and an equivalent circuit model used for the fitting the experimental data.

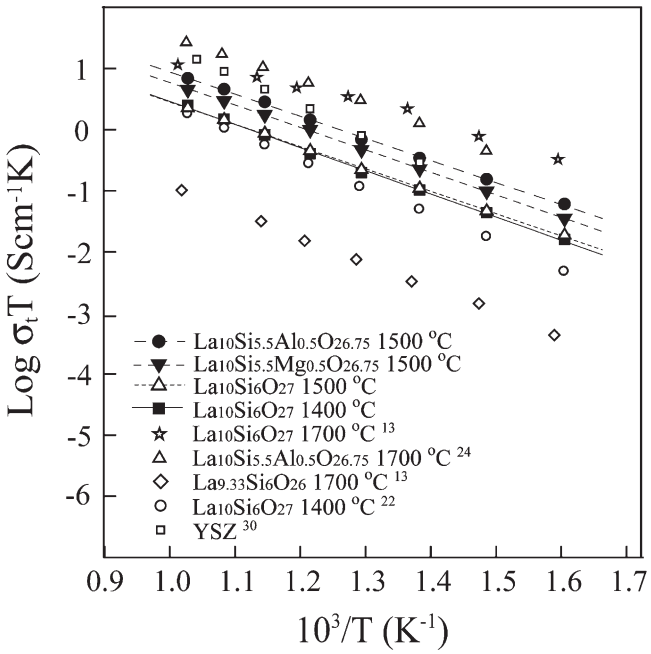

FIG. 7. Comparison of total electrical conductivity versus 1000/T plots of low-temperature-sintered undoped and doped lanthanum silicate pellets synthesized via the DEA process and calcined at 800 °C, with data on high-temperature sintered pellets reported in the literature.

TABLE II. Electrical conductivity (700 °C) and activation energy E_a data of the sintered undoped and doped lanthanum silicate pellets produced from the DEA process.

Composition	Sintering condition	E_a (eV)	σ_{total} (Scm^{-1}) at 700 °C
$La_{10}Si_6O_{27}$	1400 °C, 10 h	0.68	2.54×10^{-3}
$La_{10}Si_6O_{27}$	1500 °C, 10 h	0.66	2.33×10^{-3}
$La_{10}Si_{5.5}Al_{0.5}O_{26.75}$	1500 °C, 10 h	0.65	7.04×10^{-3}
$La_{10}Si_{5.5}Mg_{0.5}O_{26.75}$	1500 °C, 10 h	0.66	4.63×10^{-3}

of magnitude compared with the reported data obtained for $La_{10}Si_6O_{27}$[13] and $La_{10}Si_{5.5}Al_{0.5}O_{26.75}$[19] electrolytes sintered at temperatures above 1700 °C. Conversely, low-temperature-sintered undoped lanthanum silicate pellets showed much higher conductivity compared with the high-temperature sintered $La_{9.33}Si_6O_{26}$ phase electrolyte reported by Nakayama et al.,[13] which revealed that the sintered pellet is mainly composed of a highly conductive $La_{10}Si_6O_{27}$ phase. The retardation of electrical conductivity for low-temperature sintered undoped and doped lanthanum silicate pellets could be attributed to the low conductive secondary phase of $La_{9.33}Si_6O_{26}$ co-existing with the $La_{10}Si_6O_{27}$ phase.

Thus, the lanthanum silicate nanopowders that were synthesized via the DEA process and underwent low-temperature calcination could contribute to high-yield, homogenous dispersion, weak agglomeration, and desirable sintering activities. Furthermore, the parameters involved in the synthesis procedure using DEA as a participant should be modified to achieve possible enhancement of electrical conductivity for low-temperature sintered lanthanum silicate, such that it could be used as a promising solid electrolyte in IT-SOFCs.

IV. CONCLUSIONS

Nanopowders of undoped and doped lanthanum silicate apatite ceramics were successfully prepared via a DEA precipitation process. A single-phase crystalline apatite-type $La_{10}Si_6O_{27}$ was obtained using nanopowder calcined at 800 °C for 10 h. A pure crystalline $La_{10}Si_6O_{27}$ nanopowder ~30 nm in size was obtained at a relatively low calcination temperature and exhibited weak agglomeration. The $La_{10}Si_6O_{27}$ powder synthesized via the DEA process was sintered at 1400 °C with high densification. The sintering temperature

was 300 °C lower than the temperatures used in conventional sintering process. The dense grain morphological characteristics for the pellets sintered at 1400 °C for 10 h confirmed that the pellets exhibited high densification with negligible porosity. The DEA process enabled the formation of a homogenous solid solution of Al and Mg in Si sites with enhanced electrical conductivity of the doped $La_{10}Si_6O_{27}$ electrolyte, which was comparable with the YSZ electrolyte. The simple, practical and efficient DEA precipitation process resulted in a densification level above 95% in undoped and doped lanthanum silicate pellets that were sintered at a temperature of 1400–1500 °C. These temperatures were lower than the temperatures of around 1700 °C that other literature reports were used to prepare pellets via the conventional method.

ACKNOWLEDGMENTS

This work was financially supported by the Core Technology Development Program for Fuel Cells of the Ministry of Commerce, Industry, and Energy (Grant No. 10022724-2005-12), Republic of Korea, and the Korea Research Foundation Grant funded by the Korean Government (MOEHRD; KRF-2005-005-J09701).

REFERENCES

1. Z.P. Shao and S.M. Haile: A high-performance cathode for the next generation of solid-oxide fuel cells. *Nature* **431,** 170 (2004).
2. S.M. Haile: Fuel-cell materials and components. *Acta Mater.* **51,** 5981 (2003).
3. S. Hui, J. Roller, S. Yick, X. Zhang, C.D. Petit, Y. Xie, R. Maric, and D. Ghosh: A brief review of the ionic conductivity enhancement for selected oxide electrolytes. *J. Power Sources* **172,** 493 (2007).
4. B.C.H. Steele: Appraisal of $Ce_{1-y}Gd_yO_{2-y/2}$ electrolytes for IT-SOFC operation at 500 °C. *Solid State Ionics* **129,** 95 (2000).
5. N.M. Sammes, G.A. Tompsett, H. Nafe, and F. Aldinger: Bismuth based oxide electrolytes—Structure and ionic conductivity. *J. Eur. Ceram. Soc.* **19,** 1801 (1999).
6. F. Krok, I. Abrahams, D. Bangobango, W. Bogusz, and J.A.G. Nelstrop: Structural and electrical characterisation of BINIVOX. *Solid State Ionics* **111,** 37 (1998).
7. S.P. Jiang, S. Zhang, and Y.D. Zhen: Early interaction between Fe–Cr alloy metallic interconnect and Sr-doped $LaMnO_3$ cathodes of solid oxide fuel cells. *J. Mater. Res.* **20,** 747 (2005).
8. F. Mauvy, P. Lenormand, C. Lalanne, F. Ansart, J.M. Bassat, and J.C. Grenier: Electrochemical characterization of YSZ thick films deposited by dip-coating process. *J. Power Sources* **171,** 783 (2007).
9. S.P.S. Badwal and F.T. Ciacchi: Ceramic membrane technologies for oxygen separation. *Adv. Mater.* **13,** 993 (2001).
10. S.V. Chavan and A.K. Tyagi: Combustion synthesis of nanocrystalline yttria-doped ceria. *J. Mater. Res.* **19,** 474 (2004).
11. T. Ishihara, H. Matsuda, and Y. Takita: Doped $LaGaO_3$ perovskite-type oxide as a new oxide ionic conductor. *J. Am. Chem. Soc.* **116,** 3801 (1994).
12. J. Molenda, K. Swierczek, and W. Zajac: Functional materials for the IT-SOFC. *J. Power Sources* **173,** 657 (2007).
13. S. Nakayama and M. Sakamoto: Electrical properties of new type high oxide ionic conductor $RE_{10}Si_6O_{27}$ (RE = La, Pr, Nd, Sm, Gd, Dy). *J. Eur. Ceram. Soc.* **18,** 1413 (1998).
14. S. Nakayama, M. Sakamoto, M. Higuchi, K. Kodaira, M. Sato, S. Kakita, T. Suzuki, and K. Itoh: Oxide ionic conductivity of apatite type $Nd_{9.33}(SiO_4)_6O_2$ single crystal. *J. Eur. Ceram. Soc.* **19,** 507 (1999).
15. S. Nakayama and M. Sakamoto: Ionic conductivities of apatite-type $La_X(GeO_4)_6O_{1.5X-12}$ (X=8–9.33) polycrystals. *J. Mater. Sci. Lett.* **20,** 1627 (2001).
16. H. Arikawa, H. Nishiguchi, T. Ishihara, and Y. Takita: Oxide ion conductivity in Sr-doped $La_{10}Ge_6O_{27}$ apatite oxide. *Solid State Ionics* **136,** 31 (2000).
17. H. Yoshioka and S. Tanase: Magnesium doped lanthanum silicate with apatite-type structure as an electrolyte for intermediate temperature solid oxide fuel cells. *Solid State Ionics* **176,** 2395 (2005).
18. M. Higuchi, K. Kodaira, and S. Nakayama: Growth of apatite-type neodymium silicate single crystals by the floating-zone method. *J. Cryst. Growth* **207,** 298 (1999).
19. A.L. Shaula, V.V. Kharton, and F.M.B. Marques: Ionic and electronic conductivities, stability and thermal expansion of $La_{10-x}(Si,Al)_6O_{26+\delta}$ solid electrolytes. *Solid State Ionics* **177,** 1725 (2006).
20. J.E.H. Sansom, E. Kendrick, J.R. Tolchard, M.S. Islam, and P.R. Slater: A comparison of the effect of rare earth vs Si site doping on the conductivities of apatite-type rare earth silicates. *J. Solid State Electrochem.* **10,** 562 (2006).
21. I.A. Bondar: Physicochemical analysis of oxide systems based on a new class of chemical compounds-rare earth element germinates. *Inorg. Mater.* **15,** 793 (1979).
22. S.W. Tao and J.T.S. Irvine: Preparation and characterisation of apatite-type lanthanum silicates by a sol-gel process. *Mater. Res. Bull.* **36,** 1245 (2001).
23. E.J. Abram, C.A. Kirk, D.C. Sinclair, and A.R. West: Synthesis and characterisation of lanthanum germanate-based apatite phases. *Solid State Ionics* **176,** 1941 (2005).
24. Y.V. Pivak, V.V. Kharton, A.A. Yaremchenko, S.O. Yakovlev, A.V. Kovalevsky, J.R. Frade, and F.M.B. Marques: Phase relationships and transport in Ti-, Ce- and Zr-substituted lanthanum silicate systems. *J. Eur. Ceram. Soc.* **27,** 2445 (2007).
25. C. Tian, J. Liu, J. Cai, and Y. Zeng: Direct synthesis of $La_{9.33}Si_6O_{26}$ ultrafine powder via sol-gel self-combustion method. *J. Alloys Compd.* **458,** 378 (2008).
26. C. Herring: Effect of change of scale on sintering phenomena. *J. Appl. Phys.* **21,** 301 (1950).
27. D.D. Lee, S.J.L. Kang, and D.N. Yoon: Mechanism of grain growth and α–β′ transformation during liquid-phase sintering of β′-sialon. *J. Am. Ceram. Soc.* **71,** 803 (1988).
28. M.S. Kaliszewski and A.H. Heuer: Alcohol interaction with zirconia powders. *J. Am. Ceram. Soc.* **73,** 1504 (1990).
29. J.G. Li, T. Ikegami, J.H. Lee, and T. Mori: Characterization and sintering of nanocrystalline CeO_2 powders synthesized by a mimic alkoxide method. *Acta Mater.* **49,** 419 (2001).
30. M. Mori, M. Yoshikawa, H. Itoh, and T. Abe: Effect of alumina on sintering behavior and electrical-conductivity of high-purity yttria-stabilized zirconia. *J. Am. Ceram. Soc.* **77,** 2217 (1994).
31. E.J. Abram, D.C. Sinclair, and A.R. West: A novel enhancement of ionic conductivity in the cation-deficient apatite $La_{9.33}(SiO_4)_6O_2$. *J. Mater. Chem.* **11,** 1978 (2001).